

First-principles calculations on the mechanical, electronic, magnetic and optical properties of two-dimensional Janus Cr_2TeX ($X= \text{P}, \text{As}, \text{Sb}$) monolayers

Qiuyue Ma,¹ Wenhui Wan,¹ Yanfeng Ge,¹ Yingmei Li,¹ and Yong Liu^{1, a)}

State Key Laboratory of Metastable Materials Science and Technology & Key Laboratory for Microstructural Material Physics of Hebei Province, School of Science, Yanshan University, Qinhuangdao 066004, China

Janus materials possess extraordinary physical, chemical, and mechanical properties caused by symmetry breaking. Here, the mechanic properties, electronic structure, magnetic properties, and optical properties of Janus Cr_2TeX ($X= \text{P}, \text{As}, \text{Sb}$) monolayers are systematically investigated by the density functional theory. Janus Cr_2TeP , Cr_2TeAs , and Cr_2TeSb are intrinsic ferromagnetic (FM) half-metals with wide spin and half-metallic gaps. The Curie temperature (T_c) of these monolayers are about 583, 608, and 597 K, respectively by Monte Carlo simulations based on the Heisenberg model. Additionally, it has been found that Cr_2TeX ($X= \text{P}, \text{As}, \text{Sb}$) monolayers still exhibit FM half-metallic properties under biaxial strain ranging from -6% to 6%. At last, the Cr_2TeP monolayer has a higher absorption coefficient than the Cr_2TeAs and Cr_2TeSb monolayers in the visible region. The results predict that Janus Cr_2TeX ($X= \text{P}, \text{As}, \text{Sb}$) monolayers with novel properties have good potential for applications in future nanodevices.

^{a)}Electronic mail: yongliu@ysu.edu.cn

The discovery of two-dimensional (2D) honeycomb structures of graphene is considered one of the most important discoveries in the field of physics and materials science¹. The unique outstanding physical and chemical properties of graphene have led to an upsurge in the study of 2D materials. Then, a large number of 2D layered materials have been reported, including hexagonal boron nitride^{2,3}, transition metal dichalcogenides (TMDs)⁴⁻⁶, silicene⁷⁻⁹ have shown great potential for various applications. 2D Janus monolayers show novel physical and chemical properties, such as piezoelectric polarization¹⁰, Rashba effect^{11,12}, and catalytic performance^{13,14}, which open up new possibilities in the field of 2D materials. The Janus In₂SeTe is synthesized by substituting one layer of Se atoms with Te atoms to break the inversion symmetry of InSe, which possesses transport characteristics that are superior to InSe monolayer¹⁵. Similarly, the Janus In₂SSe monolayer has an indirect-direct bandgap transition due to broken vertical symmetry¹⁶. 2D Janus PdXO (X= S, Se, Te) monolayers with high electron mobility have good potential for applications in future nanodevices¹⁷. For Janus TMDs materials, the MXY (M = Mo, W; X, Y = S, Se, Te; X ≠ Y) monolayers show excellent intrinsic dipole and piezoelectric effects¹⁸.

Recently, many 2D magnetic materials have been predicted, such as CrI₃¹⁹, Cr₂Ge₂Te₆²⁰, V₃X₈²¹, Cr₂NX₂ (X = O, F, OH)²², and M₂SeTe (X= Ga, In)²³. Meanwhile, recent works also confirm that many Janus magnetic materials have excellent properties, such as Cr₂I₃X₃ (X = F, Cl, Br)²⁴, FeXY (X, Y = Cl, Br, and I, X ≠ Y)²⁵, XGaInY (X, Y;= S, Se and Te)²⁶. 2D Janus monolayers possess extraordinary physical and chemical characteristics, which have potential applications in 2D nanoscale spintronic devices. Half-metals with one spin channel conducting and the other semiconducting filter the current into a single spin channel for realizing pure spin transport, generation, and injection. The FeCl₂ is experimentally known to exist in a monolayer form and is a classical material with half-metallic properties²⁷, but its Curie temperature (T_c) is only 17 K, which greatly affects its application in spintronics due to its relatively low T_c . In recent years, it has been recognized that the half-metallic materials have exposed high T_c as a result of the strong exchange interaction driven by charge carriers²⁸. Theoretical studies have predicted many 2D half-metals with high T_c , Fe₂Si for 780 K²⁹, MnAsS₄ for 740 K³⁰, MnP and MnAs for 495 K and 711 K³¹, and Mn₂AsP monolayer for 557 K³². 2D half-metals, which have abundant charge carriers, are expected to be much higher T_c values than 2D magnetic semiconductors. The outstanding attributes of half-metals are potentially promising for the fabrication of future nanodevices.

In this work, the structural characteristics, mechanical, electronic properties, magnetic properties, and optical properties of Janus Cr_2TeX ($X = \text{P}, \text{As}, \text{Sb}$) monolayers have been studied based on the first-principles calculations. The results show that the Janus Cr_2TeX ($X = \text{P}, \text{As}, \text{Sb}$) monolayers are intrinsic ferromagnetic half-metals with wide half-metallic gaps and spin gaps. The predicted T_c of Janus Cr_2TeX ($X = \text{P}, \text{As}, \text{Sb}$) monolayers reached up to 583, 608, and 597 K. Janus Cr_2TeX ($X = \text{P}, \text{As}, \text{Sb}$) monolayers still retain their half-metallic properties and the FM natures are robust against biaxial strain in the range of -6% to 6%. At last, we displayed their optical properties, the Cr_2TeSb has a higher absorption coefficient and lower energy-loss coefficient in the ultraviolet region. Our calculations indicate that Janus Cr_2TeX ($X = \text{P}, \text{As}, \text{Sb}$) monolayers are potentially promising for spintronic devices.

The present calculations were performed by adopting the Vienna ab initio simulation package (VASP) based on the density functional theory (DFT)³³⁻³⁵. The generalized gradient approximation (GGA) functional of Perdew, Burke, and Ernzerhof (PBE) was used to investigate the exchange-correlation function³⁶. We used the spin-dependent GGA plus Hubbard U to deal with the strongly correlated interactions of the transition metal Cr element, the Hubbard U term of 3 eV was used for Cr³⁷. The plane-wave cutoff energy was chosen to be 500 eV. Monkhorst-Pack special k-point mesh is $9 \times 9 \times 1$ for the Brillouin zone integration³⁸. The convergence criteria for energy and force during the relaxation of the structures were set to 10^{-6} eV and $0.01 \text{ eV}/\text{\AA}$. The vertical vacuum spacing of 20 \AA was used to eliminate interactions between images. Phonon dispersions of the studied materials were obtained using the phonopy code based on the density functional perturbation theory (DFPT)³⁹.

The crystal structure of Janus Cr_2TeX ($X = \text{P}, \text{As}, \text{Sb}$) monolayers is shown in Fig.1(a). One Cr layer is sandwiched between the X layer and Te layer. The lattice constants of Janus Cr_2TeX monolayers increase from 4.50 of Cr_2TeP to 4.65 \AA of Cr_2TeSb due to the increase in the size of the X atom. The calculated structure parameters of Janus Cr_2TeX ($X = \text{P}, \text{As}, \text{Sb}$) monolayers are summarized in Table I. As shown in Fig.1(b), four typical magnetically coupled configurations in the $2 \times 1 \times 1$ supercell are considered to study the ground state of the Cr_2TeX ($X = \text{P}, \text{As}, \text{Sb}$) monolayers. Four spin configurations confirm that the FM coupling is more energetically stable than antiferromagnetic (AFM) coupling. Additionally, the non-magnetic state can be neglected due to the energy difference

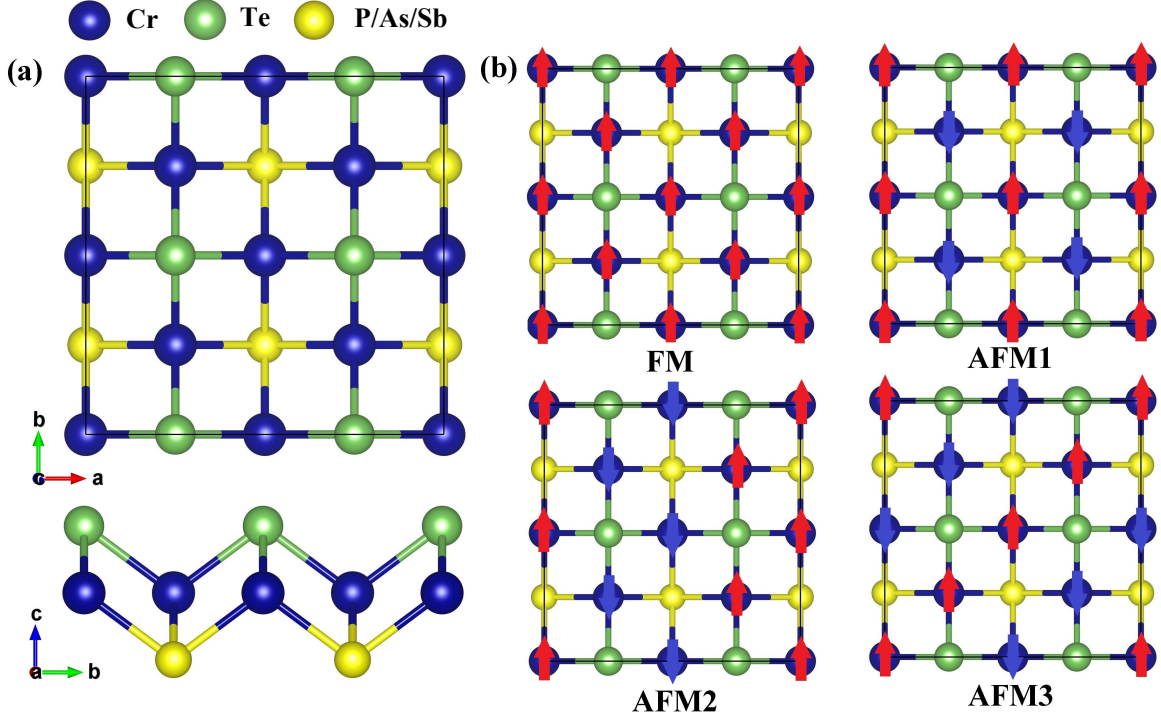


FIG. 1. (a) Top and side views of Janus Cr_2TeX ($X= \text{P}, \text{As}, \text{Sb}$) monolayers. (b) One FM and three AFM configurations of Janus Cr_2TeX ($X= \text{P}, \text{As}, \text{Sb}$) monolayers.

between the non-magnetic state and the magnetic state is too huge. In general, the magnetic state of the crystal structure is determined by the competition between two mechanisms. One is the direct AFM interaction between the nearest neighboring Cr atoms, the other is superexchange interaction among Cr-Te-Cr or Cr-X-Cr. In monolayers Cr_2TeX ($X= \text{P}, \text{As}, \text{Sb}$), the Cr-Te-Cr or Cr-X-Cr bond angles are all closer to 90° , which usually favor FM ordering according to the Goodenough-Kanamori-Anderson (GKA) rules^{40,41}. The superexchange FM dominates the total exchange interaction in Janus Cr_2TeX ($X= \text{P}, \text{As}, \text{Sb}$) monolayers due to the large Cr-Cr distance, which weakens the AFM direct exchange interaction. As a result, Janus Cr_2TeX ($X= \text{P}, \text{As}, \text{Sb}$) monolayers all adopt the FM ground state.

We then evaluated the mechanical stability of Cr_2TeX ($X= \text{P}, \text{As}, \text{Sb}$) by calculating their elastic coefficients C_{ij} . As shown in Table II, C_{ij} of Cr_2TeX decrease with increasing atomic size of X element. The elastic constants of Cr_2TeX ($X= \text{P}, \text{As}, \text{Sb}$) meet the Born criterion of stability ($C_{11}>0, C_{22}>0$ and $C_{11}-C_{12}>0$)⁴², indicating that the Cr_2TeP , Cr_2TeAs , and Cr_2TeSb are mechanically stable. In addition, the Y_{2D} of Janus Cr_2TeP , Cr_2TeAs , and

TABLE I. Lattice constants: a (Å), bond length: d_{Cr-Cr} , d_{Cr-X} , and d_{Cr-Te} (Å), the angle of Cr-Te/X-Cr : θ_1/θ_2 (°), spin gap (eV), half-metallic gap (eV), exchange constants: J_1 and J_2 (meV per Cr), magnetic anisotropy energy: MAE (μ eV per Cr), and Curie temperature: T_c (K) of Janus Cr_2TeX (X= P, As, Sb) monolayers.

System	a	d_{Cr-Cr}	d_{Cr-X}	d_{Cr-Te}	θ_1	θ_2	spin gap	half-metallic gap	J_1	J_2	MAE	T_c
Cr_2TeP	4.50	3.18	2.43	2.75	70.63	82.00	2.84	1.25	22.83	14.31	185.02	583
Cr_2TeAs	4.54	3.21	2.53	2.75	71.31	78.64	2.96	1.01	25.10	16.90	672.33	608
Cr_2TeSb	4.65	3.29	2.75	2.76	73.19	73.36	2.64	0.56	24.42	9.28	371.43	597

Cr_2TeSb monolayers were calculated to be 22.6 N/m, 16.67 N/m, and 12.88 N/m as shown in Table II. The Y_{2D} of Cr_2TeX is smaller than that of other 2D layered nanostructures, such as graphene (340 N/m)⁴³ and MoS_2 (130 N/m)⁴⁴. The small Y_{2D} proves they possess high flexibility and can sustain large strain. Furthermore, the dynamic stability was predicted by phonon dispersion calculations. The phonon spectrum of Cr_2TeX (X= P, As, Sb) without negative frequencies proves that Cr_2TeP , Cr_2TeAs and Cr_2TeSb are dynamically stable [Fig.S1].

TABLE II. Elastic constants C_{11} , C_{12} , and C_{66} (N/m), Young's modulus Y_{2D} (N/m), and Poisson's ratio ν of Janus Cr_2TeX (X= P, As, Sb) monolayers in FM state.

	C_{11}	C_{12}	C_{66}	Y_{2D}	ν
Cr_2TeP	24.47	7.69	8.39	22.06	0.31
Cr_2TeAs	17.20	3.01	7.10	16.67	0.17
Cr_2TeSb	13.25	2.21	5.52	12.88	0.16

Fig.2(a)-(f) shows the band structures of Cr_2TeX at the PBE level. Notably, the spin-up bands cross the Fermi level, while the spin-down channel acts as a semiconductor, indicating that they are intrinsic half-metals. The calculated electronic band structures of the Cr_2TeX

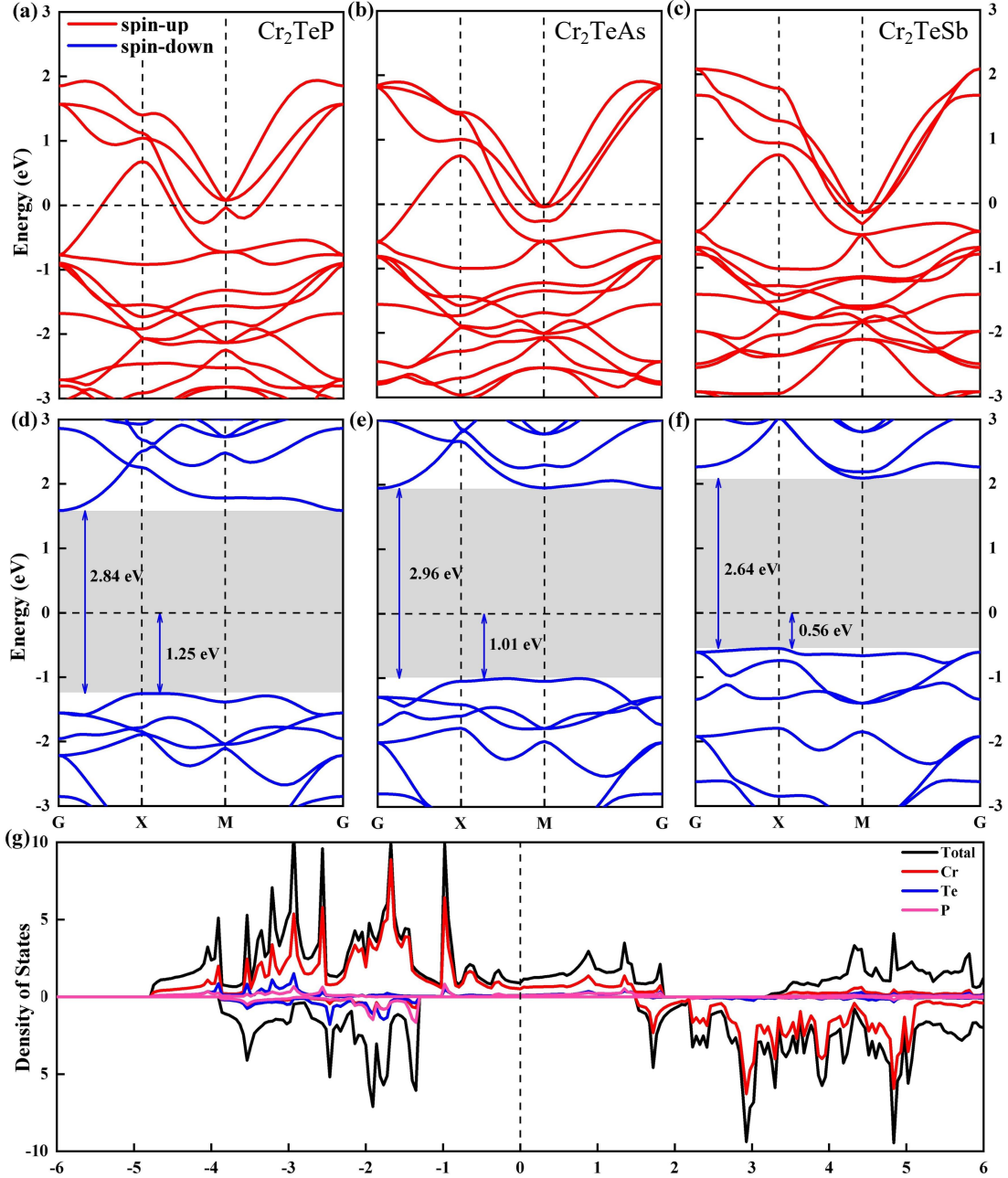


FIG. 2. The electronic band structures of Cr₂TeP (a,d), Cr₂TeAs (b,e), and Cr₂TeSb (c,f). The total density of states (TDOS) and projected density of states (PDOS) of Cr₂TeP monolayer (g).

exhibit half-metallic gaps ranging from 1.25 eV of Cr₂TeP to 0.56 eV of Cr₂TeSb, which can effectively prevent thermally excited spin-flip transitions. The band gaps on the spin-down channel were 2.84, 2.96, and 2.64 eV for Cr₂TeP, Cr₂TeAs, and Cr₂TeSb at the PBE levels, respectively, which is beneficial for the spin-polarized carrier injection and detection.

Because the PBE functional tends to underestimate the band gap, the HSE06 functional was used to correct the band structures, which showed the band gaps in the spin-down channel increased to 3.70, 3.84, and 3.53 eV for the Cr₂TeP, Cr₂TeAs, and Cr₂TeSb monolayers, respectively. In the partial density of states (PDOS) of Cr₂TeX [Fig.2(g) and Fig.S2], the spin-up electronic states near the Fermi level are mainly contributed by Cr atoms. For the spin-down electronic states, the conduction band minimum is mainly contributed by Cr atoms, while the Cr, X, and Te atoms all contribute to the valence band maximum.

To estimate the T_c of Janus Cr₂TeX (X= P, As, Sb) monolayers, we performed Monte carlo simulations based on the Heisenberg model with the Hamiltonian of:

$$H = - \sum_{\langle ij \rangle} J_1 S_i S_j - \sum_{\langle ik \rangle} J_2 S_i S_k - A S_i^Z S_i^Z \quad (1)$$

Where J_1 and J_2 are the exchange constants, S_i and S_j are the spin operators on sites i and j , respectively. S_i^Z is the spin parallel to the Z direction. And A is the magnetic anisotropy energy parameter (MAE). J_1 and J_2 can be obtained by equations:

$$E_{FM} = E_0 - 2J_1 S^2 - 2J_2 S^2 - A S^2 \quad (2)$$

$$E_{AFM1} = E_0 + 2J_1 S^2 - 2J_2 S^2 - A S^2 \quad (3)$$

$$E_{AFM3} = E_0 + 2J_2 S^2 - A S^2 \quad (4)$$

The calculated J_1 , J_2 , and MAE are listed in Table I. As shown in Fig.3, T_c are estimated to be 583, 608, and 597 K for the Cr₂TeP, Cr₂TeAs, and Cr₂TeSb, respectively, much higher than those in the 2D FM half-metals reported early, e.g., FeClBr (28 K), FeClI (21 K), FeBrI (29 K)²⁵, ScCl (185 K)⁴⁵, and VSeTe (350 K)⁴⁶. The Janus Cr₂TeP, Cr₂TeAs, and Cr₂TeSb with high T_c are benefit for possible applications in spintronic devices.

Then, we study the effects of biaxial strain on the electronic and magnetic properties of Cr₂TeX (X= P, As, Sb) monolayers. As shown in Fig.4(a), the energy difference between the FM and AFM configurations under the biaxial strain indicates that no phase transition occurs during the process of biaxial strain and FM is always the ground state. And the energy difference of Cr₂TeAs and Cr₂TeSb increases with the increase in tensile strain and decreases with the compressive strain. The half-metallic gaps in the Janus of Cr₂TeP and Cr₂TeAs

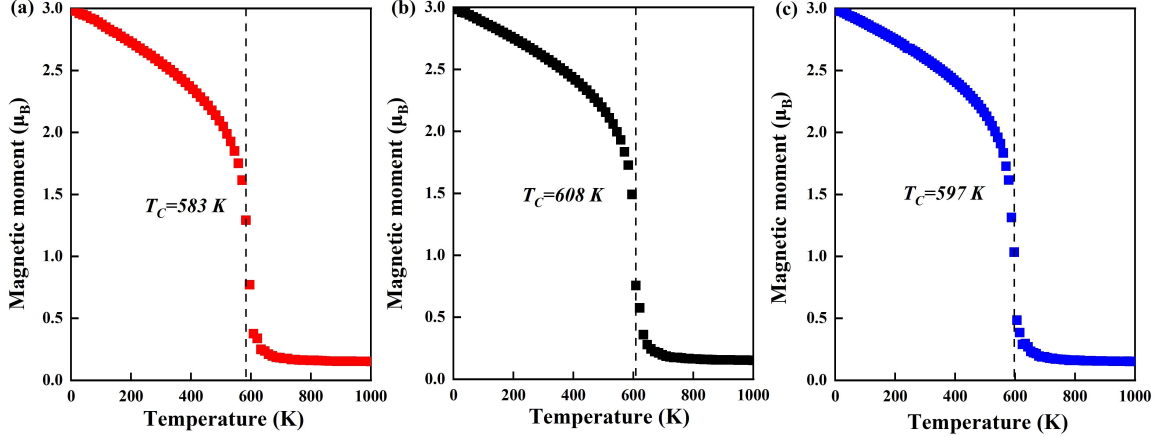


FIG. 3. On-site magnetic moment of Cr atoms versus temperature in Cr_2TeP (a), Cr_2TeAs (b), and Cr_2TeSb (c).

monolayers monotonously decrease as biaxial strain increases from -6% to 6% [Fig.4(b)]. Meanwhile, the half-metallic gap of Cr_2TeP reaches a maximum value under 2% strain. When biaxial strain of -2%, 0%, and 2% are applied for Cr_2TeP , Cr_2TeAs , and Cr_2TeSb , respectively, the spin gaps reach the maximum value of 2.98, 2.96, and 2.83 eV [Fig.4(c)].

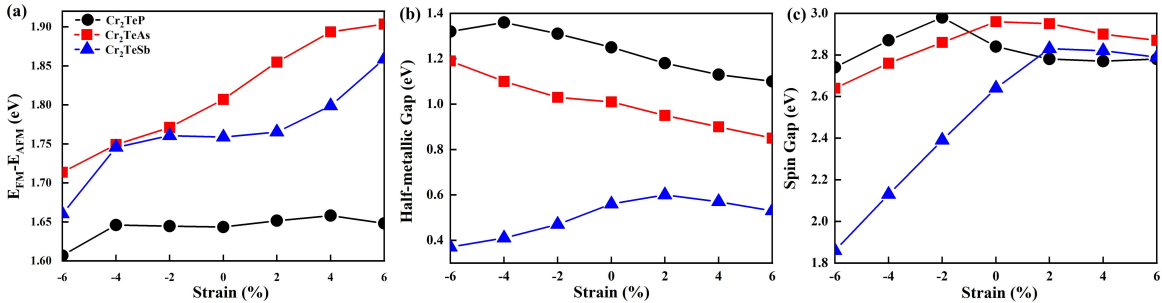


FIG. 4. Energy difference (a) between the FM and AFM phases, variation of the half-metallic gap (b) and spin gap (c) under biaxial strain for Janus Cr_2TeP , Cr_2TeAs , and Cr_2TeSb .

At last, we investigated the optical properties of Cr_2TeX ($X = \text{P}, \text{As}, \text{Sb}$) monolayers by including the photon absorption coefficient $\alpha(\omega)$, energy-loss coefficient $L(\omega)$, reflectivity $R(\omega)$, and refraction coefficient $n(\omega)$. As shown in Fig.5(a), in the energy range of 0-5 eV, the overall absorption coefficient of Cr_2TeX monolayers show a gradually increasing trend. The absorption coefficient in the visible range (1.3-3.5 eV) is higher in Cr_2TeP monolayer than in the Cr_2TeAs and Cr_2TeSb monolayers as a result of the higher $\alpha(\omega)$ of the Cr_2TeP

monolayer in this range. In the ultraviolet region (3.5-5 eV), Cr₂TeSb shows a higher $\alpha(\omega)$. Fig.5(b) shows that $L(\omega)$ of the Cr₂TeSb is fairly low in the visible range (1.3-3.5 eV), and its $L(\omega)$ is also significantly lower than that of the Cr₂TeAs and Cr₂TeSb monolayers in the ultraviolet region (3.5-5 eV). The lower $L(\omega)$ indicates that the Cr₂TeSb monolayer has favorable photon transmittance. The refraction coefficient can be used to characterize the attenuation of light energy. We can see that Cr₂TeSb monolayer has a higher reflectivity $R(\omega)$ in the infrared region (0.6-1.3 eV)[Fig. 5(c)(d)]. The higher the refraction coefficient, the more the incident, and the higher the ability of light to be refracted. The overall trend of the refraction coefficient of Cr₂TeX monolayers is gradually decreasing. In the infrared region of photon energy 0-1.3 eV, the refraction coefficient decays rapidly, and the Cr₂TeP has a higher $n(\omega)$ than the other two monolayers. In the visible range of 1.3-3.5 eV, the refraction coefficient tends to weaken with the decay of the incident light energy, and the decay tends to level off in the ultraviolet region at 3.5-5.0 eV, and the difference in refractive power with Cr₂TeX in the ultraviolet region is not significant.

In conclusion, the structural, mechanical, electronic, magnetic, and optical properties of Janus Cr₂TeX (X= P, As, Sb) monolayers have been studied by means of DFT calculations. The calculated results demonstrated that all three structures of Cr₂TeX were found to be mechanically and dynamically stable. We have predicted that the Janus Cr₂TeX monolayers are large band gap FM half metals. Meanwhile, we further reveal that Cr₂TeX (X= P, As, Sb) show a high T_c about 583, 603, and 597 K, respectively. The FM half-metallic characteristics can exist stably in a large strain range from -6% to 6%. The optical properties show that Cr₂TeSb has higher absorption coefficient and lower energy-loss coefficient in the ultraviolet region. The present results indicate that these Janus Cr₂TeX (X= P, As, Sb) monolayers have potential functional materials for spintronic applications and enrich the 2D Janus half-metallic material library.

Supplementary Material includes 2 figures.

This work was supported by the Innovation Capability Improvement Project of Hebei province (No. 22567605H), the Natural Science Foundation of Hebei Province of China (No. A2022203006), the Science and Technology Project of Hebei Education Department (No. BJK2022002 and QN2023177). The numerical calculations in this paper have been done on the supercomputing system in the High Performance Computing Center of Yanshan University.

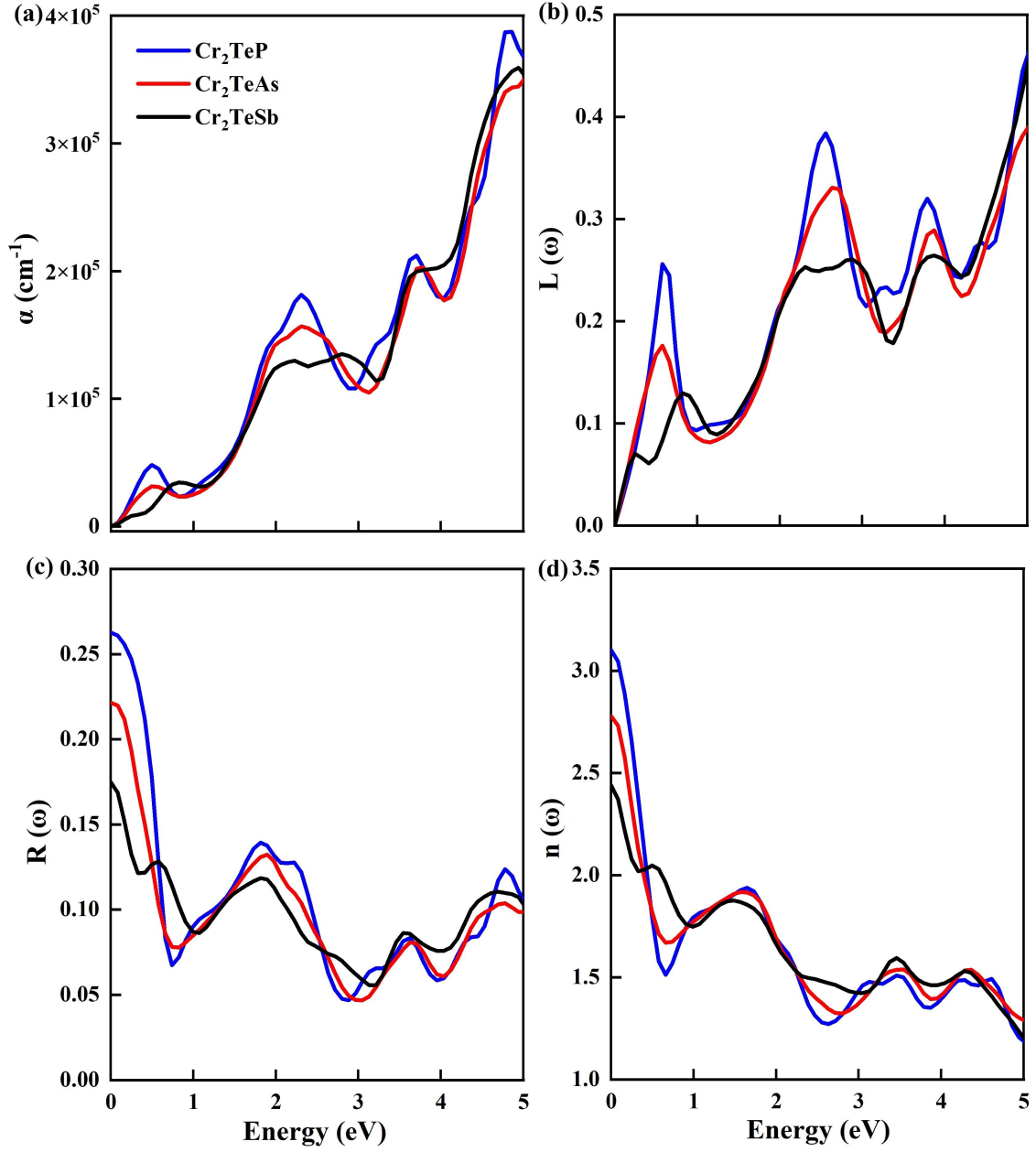


FIG. 5. Optical property diagram of Cr₂TeX (X= P, As, Sb) monolayers: photon absorption coefficient (a), energy-loss coefficient (b), reflectivity (c), and refraction coefficient (d).

I. DATA AVAILABILITY

The data that support the findings of this study are available from the corresponding author upon reasonable request.

II. REFERENCES

REFERENCES

- ¹K. S. Novoselov, A. K. Geim, S. V. Morozov, D. Jiang, Y. Zhang, S. V. Dubonos, I. V. Grigorieva, and A. A. Firsov, "Electric Field Effect in Atomically Thin Carbon Films," [Science](#) **306**, 666 (2004).
- ²K. Novoselov, D. Jiang, F. Schedin, T. Booth, V. Khotkevich, S. Morozov, and A. Geim, "Two Dimensional Atomic Crystals," [Proc. Natl. Acad. Sci. U. S. A.](#) **102**, 10451 (2005).
- ³C. Jin, F. Lin, K. Suenaga, and S. Iijima, "Fabrication of a Freestanding Boron Nitride Single Layer and Its Defect Assignments," [Phys. Rev. Lett.](#) **102**, 195505 (2009).
- ⁴M. Chhowalla, H. S. Shin, G. Eda, L. J. Li, K. P. Loh, and H. Zhang, "The chemistry of two-dimensional layered transition metal dichalcogenide nanosheets," [Nat. Chem.](#) **5**, 263 (2013).
- ⁵K. F. Mak, C. Lee, J. Hone, J. Shan, and T. F. Heinz, "Atomically Thin MoS₂: A New Direct-Gap Semiconductor," [Phys. Rev. Lett.](#) **105**, 136805 (2010).
- ⁶A. Splendiani, L. Sun, Y. B. Zhang, T. S. Li, J. Kim, C. Y. Chim, G. Galli, and F. Wang, "Emerging Photoluminescence in Monolayer MoS₂," [Nano Lett.](#) **10**, 1271 (2010).
- ⁷B. Lalmi, H. Oughaddou, H. Enriquez, A. Kara, S. Vizzini, B. Ealet, and B. Aufray, "Epitaxial growth of a silicene sheet," [Appl. Phys. Lett.](#) **97**, 223109 (2010).
- ⁸S. Wu, G. Shan, and B. Yan, "Prediction of Near-Room-Temperature Quantum Anomalous Hall Effect on Honeycomb Materials," [Phys. Rev. Lett.](#) **113**, 256401 (2014).
- ⁹M. Yang, X. Zhang, and W. Liu, "Tunable topological quantum states in three- and two-dimensional materials," [Front. Phys.](#) **10**, 161 (2015).
- ¹⁰C. Zhang, Y. Nie, S. Sanvito, and A. Du, "A First-Principles Prediction of a Room-Temperature Ferromagnetic Janus VSSe Monolayer with Piezoelectricity, Ferroelasticity, and Large Valley Polarization," [Nano Lett.](#) **19**, 1366 (2019).
- ¹¹Q. Yao, J. Cai, W. Tong, S. Gong, J. Wang, X. Wan, C. Duan, and J. H. Chu, "Manipulation of the large Rashba spin splitting in polar two-dimensional transition-metal dichalcogenides," [Phys. Rev. B](#) **95**, 165401 (2017).
- ¹²T. Hu, F. Jia, G. Zhao, J. Wu, A. Stroppa, and W. Ren, "Intrinsic and anisotropic Rashba spin splitting in Janus transition-metal dichalcogenide monolayers," [Phys. Rev. B](#)

- 97**, 235404 (2018).
- ¹³D. Er, H. Ye, N. C. Frey, H. Kumar, J. Lou, and V. B. Shenoy, "Prediction of Enhanced Catalytic Activity for Hydrogen Evolution Reaction in Janus Transition Metal Dichalcogenides," *Nano Lett.* **18**, 3943 (2018).
- ¹⁴X. Ma, X. Wu, H. Wang, and Y. Wang, "A Janus MoSSe monolayer: a potential wide solar-spectrum water-splitting photocatalyst with a low carrier recombination rate," *J. Mater. Chem. A* **6**, 2295 (2018).
- ¹⁵W. Wan, S. Zhao, Y. Ge, and Y. Liu, "Phonon and electron transport in Janus monolayers based on InSe," *J. Phys.: Condens. Matter* **31**, 435501 (2019).
- ¹⁶A. Kandemir and H. Sahin, "Janus single layers of In₂SSe: A first-principles study," *Phys. Rev. B* **97**, 155410 (2018).
- ¹⁷T. V.Vu, H. V.Phuc, S. Ahmad, B. D.Hoi, N. V.Hieu, S. Al-Qaisi, A. I.Kartamyshev, and N. N.Hieu, "Theoretical prediction of Janus PdXO (X = S, Se, Te) monolayers: structural, electronic, and transport properties," *RSC Adv.* **12**, 12971 (2022).
- ¹⁸L. Dong, J. Lou, and V. B. Shenoy, "Large In-Plane and Vertical Piezoelectricity in Janus Transition Metal Dichalcogenides," *ACS Nano* **11**, 8242 (2017).
- ¹⁹B. Huang, G. Clark, E. Navarro-Moratalla, D. R. Klein, R. Cheng, K. L. Seyler, D. Zhong, E. Schmidgall, M. A. McGuire, D. H. Cobden, W. Yao, D. Xiao, P. Jarillo-Herrero, and X. X-u, "Layer-dependent ferromagnetism in a van der Waals crystal down to the monolayer limit," *Nature* **546**, 270 (2017).
- ²⁰C. Gong, L. Li, Z. Li, H. Ji, A. Stern, Y. Xia, T. Cao, W. Bao, C. Wang, Y. Wang, Z. Q. Qiu, R. J. Cava, S. G. Louie, J. Xia, and X. Zhang, "Discovery of intrinsic ferromagnetism in two-dimensional van der Waals crystals," *Nature* **546**, 265 (2017).
- ²¹H. Xiao, X. Wang, R. Wang, L. Xu, S. Liang, and C. Yang, "Intrinsic magnetism and biaxial strain tuning in two-dimensional metal halides V₃X₈ (X= F, Cl, Br, I) from first principles and Monte Carlo simulation," *Phys. Chem. Chem. Phys.* **21**, 11731 (2019).
- ²²Q. Sun, J. Li, Y. Li, Z. Yang, and R. Wu, "Cr₂NX₂ MXene (X = O, F, OH): A 2D ferromagnetic half-metal," *Appl. Phys. Lett.* **119**, 062404 (2021).
- ²³Y. Guo, S. Zhou, Y. Bai, and J. Zhao, "Enhanced piezoelectric effect in Janus group-III chalcogenide monolayers," *Appl. Phys. Lett.* **110**, 163102 (2017).
- ²⁴W. Qin, G. Wang, B. Xu, B. Sun, G. Liu, "Element-dependent unique properties of Janus Cr₂I₃X₃ (X = F, Cl, Br) monolayer: Insight from first-principles calculations," *Mater. Sci.*

- [Eng. B 278](#), 115610 (2022)
- ²⁵R. Li, J. Jiang, X. Shi, W. Mi, and H. Bai, "Two-Dimensional Janus FeXY (X, Y = Cl, Br, and I, X \neq Y) Monolayers: Half-Metallic Ferromagnets with Tunable Magnetic Properties under Strain," [ACS Appl. Mater. Interfaces](#) **13**, 38897 (2021)
- ²⁶I. AhMaD, I. Shahid, A. Ali, L. Gao, and J. Cai, "Electronic, mechanical, optical and photocatalytic properties of two-dimensional Janus XGaInY (X, Y = S, Se and Te) monolayers," [RSC Adv.](#) **11**, 17230 (2021)
- ²⁷E. Torun, H. Sahin, S. K. Singh, and F. M. Peeters, "Stable half-metallic monolayers of FeCl₂" [Appl. Phys. Lett.](#) **106**, 192404 (2015).
- ²⁸C. Zener, "Interaction between the d-Shells in the Transition Metals. II. Ferromagnetic Compounds of Manganese with Perovskite Structure," [Phys. Rev.](#) **82**, 403 (1951)
- ²⁹Y. Sun, Z. Zhuo, X. Wu, J. Yang, "Room-Temperature Ferromagnetism in Two-Dimensional Fe₂Si Nanosheet with Enhanced Spin-Polarization Ratio," [Nano Lett.](#) **17**, 2771 (2017)
- ³⁰T. Hu, W. Wan, Y. Ge, and Y. Liu, "Robust intrinsic half-metallic ferromagnetism in stable 2D single-layer MnAsS₄," [J. Phys.: Condens. Matter](#) **32**, 385803 (2020)
- ³¹B. Wang, Y. Zhang, L. Ma, Q. Wu, Y. Guo, X. Zhang, and J. Wang, "MnX (X=P, As) Monolayers: A New Type of Two-dimensional Intrinsic Room Temperature Ferromagnetic Half-Metallic Materials with Large Magnetic Anisotropy," [Nanoscale](#) **11**, 4204 (2019)
- ³²H. Zeng, S. Jin, J. Wang, Y. Hu, and X. Fan, "Ferromagnetic half-metal with high Curie temperature: Janus Mn₂PAs monolayer," [J. Mater. Sci.](#) **56**, 13215 (2021)
- ³³P. E. Blöchl, "Projector augmented-wave method" [Phys. Rev. B](#) **50**, 17953 (1994).
- ³⁴G. Kresse and J. Furthmüller, "Efficient iterative schemes for ab initio total-energy calculations using a plane-wave basis set" [Phys. Rev. B](#) **54**, 11169 (1996).
- ³⁵G. Kresse and J. Furthmüller, "Efficiency of ab-initio total energy calculations for metals and semiconductors using a plane-wave basis set" [Comput. Mater. Sci.](#) **6**, 15 (1996).
- ³⁶J. P. Perdew, K. Burke, and M. Ernzerhof, "Generalized gradient approximation made simple" [Phys. Rev. Lett.](#) **77**, 3865 (1996).
- ³⁷A. I. Liechtenstein, V. I. Anisimov, and J. Zaanen, "Density-functional theory and strong interactions: Orbital ordering in Mott-Hubbard insulators" [Phys. Rev. B](#) **52**, R5467 (1995).
- ³⁸H. J. Monkhorst and J. D. Pack, "Special points for Brillouin zone integrations" [Phys. Rev. B](#) **13**, 5188 (1976).

- ³⁹S. Baroni, S. de Gironcoli, A. Dal Corso, and P. Giannozzi, "Phonons and related crystal properties from density-functional perturbation theory" *Rev. Mod. Phys.* **73**, 515 (2001).
- ⁴⁰J. B. Goodenough, "Theory of the role of covalence in the perovskite-type manganites [La,M(II)] MnO₃" *Phys. Rev.* **100**, 564 (1955).
- ⁴¹J. Kanamori, "Crystal distortion in magnetic compounds" *J. Appl. Phys.* **31**, S14 (1960).
- ⁴²Z. Wu, E. Zhao, H. Xiang, X. Hao, X. Liu, and J. Meng, "Crystal structures and elastic properties of superhard IrN₂ and IrN₃ from first principles" *Phys. Rev. B* **76**, 054115 (2007).
- ⁴³D. G. Papageorgiou, I. A. Kinloch and R. J. Young, "Mechanical properties of graphene and graphene-based nanocomposites" *Prog. Mater. Sci.* **90**, 75 (2017).
- ⁴⁴R. C. Cooper, C. Lee, C. A. Marianetti, X. Wei, J. Hone and J. W. Kysar, "Nonlinear elastic behavior of two-dimensional molybdenum disulfide" *Phys. Rev. B* **87**, 035423 (2013).
- ⁴⁵B. Wang, Q. Wu, Y. Zhang, Y. Guo, X. Zhang, Q. Zhou, S. Dong, and J. Wang, "High Curie-Temperature Intrinsic Ferromagnetism and Hole Doping-Induced Half-Metallicity in Two-Dimensional Scandium Chlorine Monolayer," *Nanoscale Horiz.* **3** 551 (2018).
- ⁴⁶Z. Guan and S. Ni, "Predicted 2D ferromagnetic Janus VSeTe monolayer with high Curie temperature, large valley polarization and magnetic crystal anisotropy," *Nanoscale* **12** 22735 (2020).